WALAILAK JOURNAL
http://wjst.wu.ac.th Engineering and Physical Sciences

# Electrical Characterization by Impedance Spectroscopy of Double Perovskites of $Y_2NiMnO_6$ Ceramics

**Thanapong SAREEIN[1] and Naphat ALBUTT[1,2,*]**

[1]*Division of Industrial Materials Science, Faculty of Science and Technology, Rajamangala University of Technology Phra Nakhon, Bangkok 10800, Thailand*
[2]*Advanced Materials Physics Laboratory (Amp.), School of Physics, Institute of Science, Suranaree University of Technology, Nakhon Ratchasima 30000, Thailand*

**([*]Corresponding author's e-mail: naphat.cha@rmutp.ac.th)**

*Presented at 41st Congress on Science and Technology of Thailand: November 6th - 8th 2015*
*Full paper accepted: 2 March 2016*

**Abstract**

Impedance spectroscopy was used in order to investigate the electric properties of double perovskites of the $Y_2NiMnO_6$ ceramics, which were prepared by thermal decomposition at 800 °C for 6 h followed by sintering at 1400 °C for 6, 12, 18 and 24 h. Consequently, the electric characterization of the $Y_2NiMnO_6$ ceramics was performed at temperature from −50 to 200 °C, in the frequency range from $10^2$ to $10^8$ Hz. Results in the activation energy relaxation ($Ea_{(\tau g)}$) are significantly increased from 0.1723 to 0.3813 eV and the conductivity activation energy ($Ea_{(\sigma gb)}$) in the grain boundary are dramatically increased from approximately 0.3599 to 0.6260 eV at 24 h. Dispersion was observed in the variation of impedance values with frequency. Possible reasons for these observations are discussed.

**Keywords:** Impedance, dielectric, perovskites, grain size

## Introduction

Microelectronics devices are continuously developed for industrial revolution. In addition, devices are becoming miniaturized, consuming less power, and with reduced cost of manufacture, but they have powerful options and the best security in use. Ceramics have desirable properties for electronic capacitors including the highest dielectric permittivity over the performed period, lowest dielectric loss tangent [1,2] and perform with several frequencies and at many temperatures. However, the giant dielectric materials are selected to probe the various properties. Even though many dielectric materials have been investigated by several researchers [3-8], perovskites materials such as $BiFeO_3$ and $YMnO_3$, play an important role as a structure for most multiferroic compounds. Thus, almost all perovskites have a high dielectric constant. The $Y_2NiMnO_6$ materials exhibit magnetic and dielectric properties similar in behavior to double perovskite with an electric field and various temperatures [9-11]. Another important point for such ceramics is that the dielectric behavior and activation energy for $Y_2NiMnO_6$ are comparable to that of charge ordered $La_2NiMnO_6$ [12,13]. In particular, the activation energy is close to the energy required to transfer an electron from $Ni^{2+}$ to $Mn^{4+}$ and there are sufficient values to substitute the direction of the polar region, indicating that the conformable dielectric characteristics in $Y_2NiMnO_6$ may be ascribed to the charge ordering [14-16]. However, charge ordered perovskite materials, which exhibit this type of ferroelectricity are of interest to many researchers and industrial factories, both theoretically and experimentally [17-22]. Consequently, the ceramic materials $Y_2NiMnO_6$ are investigated by exploring the fundamental understanding of the $Ni^{2+}$–O–$Mn^{4+}$ electronic interaction inside the structure.

In this research, we successfully prepared $Y_2NiMnO_6$ powder by a thermal decomposition method and it was sintered by high temperature at 1400 °C several sintering times (6, 12, 18 and 24 h) [23]. The study investigated the formation for $Y_2NiMnO_6$ ceramics under a variety of conditions. The samples of the $Y_2NiMnO_6$ ceramics were characterized by X-ray diffraction (XRD) to investigate of pattern phase and scanning electron microscopy (SEM) for surface morphologies. Lastly, the dielectric properties were measured, including impedance (Z), dielectric permittivity ($\varepsilon'$), dielectric loss ($\varepsilon''$) and loss tangent (tanδ) at temperature range −50 to 200 °C by using an Agilent 4294 A (Precision Impedance Analyzer).

## Materials and methods

The bulk $Y_2NiMnO_6$ sample was synthesized using $Y(CH_3COO)_3.xH_2O$ (Yttrium (III)acetate hydrate, 99.9 %), $Ni(CH_3COO)_2.4H_2O$ (Nickel (II)acetate tetrahydrate, 99.0 %) and $Mn(CH_3COO)_2.4H_2O$ (Manganese (II)acetate tetrahydrate, 99.0 %), mixed in deionized (DI) water (1:7.5). For the experimental part, the mixtures were stirred at room temperature overnight in order to yield a homogeneous solution. Firstly, the solution was heated in air from 100 to 800 °C for 11 h and then at 800 °C for 6 h to obtain the powder for sintering. Secondly, the sample was sintered at a rate of 5 °C/min until 1400 °C and maintained at that temperature 6, 12, 18 and 24 h, respectively.

To reveal the phase composition and microstructure, the bulk $Y_2NiMnO_6$ and sintered ceramics were characterized by X-ray diffraction (XRD) (Bruker D8 HRXRD, Germany) and scanning electron microscopy (SEM) (JEOL JSM-6010, Resolution 5.0 nm in LV mode). It is important to note that using the XRD patterns confirm to main phase of $Y_2NiMnO_6$ ceramics with several sintering times were reported by JCPDS card. In the electrical characterization, the ceramic samples were given electrical contacts by silver painting on both sides of the disk shaped samples, and they were allowed to dry overnight. Finally, the electric response of the sample was measured using an Agilent 4294A (frequency range 40 Hz to 110 MHz) Precision Impedance Analyzer which was used by a frequency ranging from $10^2$ to $10^8$ Hz and oscillation voltage of 1.0 V. The measurements were performed from 200 to −50 °C. Furthermore, each measured temperature was kept constant with an accuracy of ±1K.

## Results and discussion

### XRD and SEM for $Y_2NiMnO_6$ ceramics

XRD at high temperature demonstrates that the ceramic material groups have a structure consistent with the general literature. The diffraction peaks shown in **Figure 1** can be assigned to a monoclinic cell with a $P2_{1/n}$ space group, which is typical for a ceramics material with charge ordering (1:1) of the Ni and Mn cations. According to diffraction peaks, the samples that were sintered at high temperature clearly gave a main phase at several positions. The sintered samples show an increased (111) phase in comparison to the bulk, with highest contribution at 18 h. The main (112) phase was highest after 12 h of sintering, which can explain in part the different electrical properties of these ceramics.

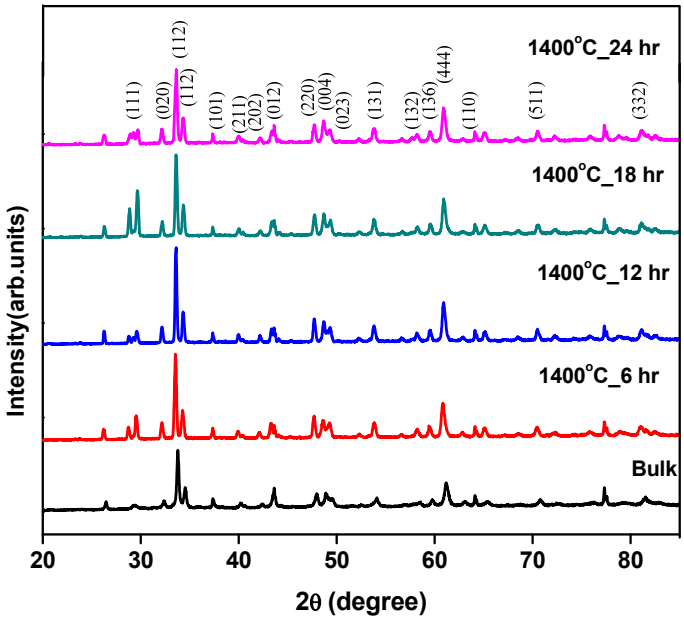


**Figure 1** XRD spectra of $Y_2NiMnO_6$ bulk (non-sintered) and $Y_2NiMnO_6$ ceramics sintered at 1400 °C for 6, 12, 18 and 24 h, respectively.

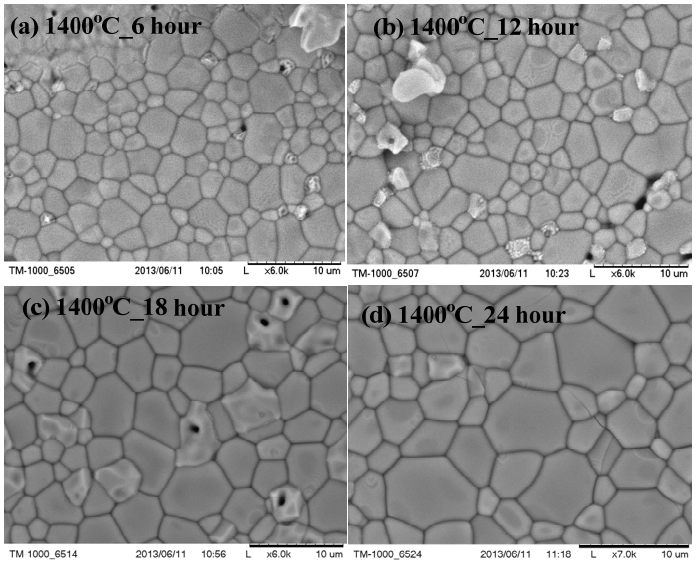


**Figure 2** SEM images of the surface morphologies of the $Y_2NiMnO_6$ ceramics sintered at 6, 12, 18 and 24 h.

The resulting SEM images show significant changes in microstructure with sintering time. The sample sintered for 6 h shows a fine-grained microstructure with average grain sizes of approximately 1.36 µm, grain boundary of about 0.179 µm and the largest grain sizes of ~4.82 µm, as shown in **Figure**

**2(a)**. As seen in **Figure 2(b)**, the sample $Y_2NiMnO_6$ ceramics at 12 h exhibits non fine-grained microstructure with average grain sizes of ~1.56 µm, grain boundary of about 0.137 µm and the biggest grain sizes of ~6.91 µm. Surprisingly, the $Y_2NiMnO_6$ ceramics sintered for 18 h indicates some grains were distorted and appeared porous, which was attributed to the value of average grain sizes of ~ 3.36 µm, grain boundary of ~0.191 µm and the highest size of ~8.16 µm for dense microstructure, as shown in **Figure 2(c)**. Finally, the sample sintered for 24 h exhibits high performance grain sizes at ~10.23 µm, average grain sizes of ~5.24 µm and grain boundary sizes at about 0.21 µm, as seen in **Figure 2(d)**. It was observed that the grain size increased moderately from 1.36 after 6 h to 1.5 µm after 12 h, while longer sintering times demonstrated a greater range of grain sizes. These results will help explain the dielectric properties. The information concerning grain size and grain boundary size were obtained with Image-Pro Plus5.1.

**Impedance spectroscopy**

Impedance spectroscopy is an important measurement to study the electrical properties of ceramic materials, presenting electrically inhomogeneous structure and properties of ceramic materials [24-26]. It can be used to separately study the electrical responses of the conducting part and insulating part of the ceramic materials. The complex impedance ($Z^*$) of a ceramic material can be obtained from the parameter $Z^* = V^*/I^*$, where $V^*$ is the applied voltage and $I^*$ is the measuring current. Nevertheless, the parameter $Z^*$ can be investigated from the complex dielectric constant ($\varepsilon^*$), from $Z^* = 1/j\omega C_0\varepsilon^*$, where $\varepsilon^*$ is found from $\varepsilon^* = \varepsilon' - j\varepsilon''$. Consequently, the parameters $\varepsilon'$ and $\varepsilon''$ are presented for the real part and imaginary part of the complex permittivity. Normally, $\omega$ is the angular frequency ($\omega = 2\pi f$) and $C_0 = \varepsilon_0 A/d$ is the empty cell capacitance of ceramic materials, A is the sample area and d is the ceramic thickness. An outstanding parameter is that the values of ac conductivity ($\sigma_{ac}$) which is calculated from $\sigma_{ac} = \varepsilon_0\omega\varepsilon''$. In addition, the complex impedance $Z^*$ of the ceramic materials can be modeled by ideal equivalent circuits that have resistors R and capacitors C for investigating the electrical property of the sample. However, there is more than one electrical response in the ceramic material. Interestingly, these ceramic materials display grain boundary impedance ($R_{gb}, C_{gb}$) in addition to grain ($R_g, C_g$) effects [25], which can be represented by the equivalent circuit shown in **Figure 3**.

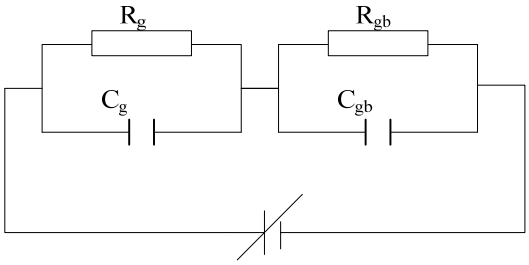


**Figure 3** Equivalent circuit used to represent the electrical properties of a polycrystalline ceramic material that demonstrates grain ($R_g$, $C_g$) and grain boundary ($R_{gb}$, $C_{gb}$) effects.

As shown in **Figure 3**, the equivalent circuit consists of 2 parts, with the first part representing grain effects ($R_g$, $C_g$) and the second part representing grain boundaries ($R_{gb}$, $C_{gb}$). The circuit consists of a resistor (R) and capacitor (C) joined in parallel. Accordingly, the electrical properties response from the grain boundary should be associated with larger resistance ($R_{gb}$) and capacitance ($C_{gb}$) than those of grains ($R_g$, $C_g$). Grain boundary's ($R_{gb}$, $C_{gb}$) response frequency is therefore much lower than that of the grain ($R_g$, $C_g$), and it gives rise to a relatively strong peak in the impedance in ceramic materials.

$$Z^* = Z' - jZ'' = \frac{1}{R_g^{-1}+j\omega C_g} + \frac{1}{R_{gb}^{-1}+j\omega C_{gb}} \quad (1)$$

where the real part ($Z'$) and imaginary part ($Z''$) of the complex impedance ($Z^*$) for impedance of ceramic materials, it can be separated for 2 equations;

$$Z' = \frac{R_g}{1+(\omega R_g C_g)^2} + \frac{R_{gb}}{1+(\omega R_{gb} C_{gb})^2} \quad (2)$$

$$Z'' = R_g\left[\frac{\omega R_g C_g}{1+(\omega R_g C_g)^2}\right] + R_{gb}\left[\frac{\omega R_{gb} C_{gb}}{1+(\omega R_{gb} C_{gb})^2}\right] \quad (3)$$

where the resistances ($R_g$, $R_{gb}$) and the capacitances ($C_g$, $C_{gb}$) represent the grains and grain boundaries, respectively.

$$Z^* = \frac{R_{gb}}{1+j\omega R_{gb} C_{gb}} \quad (4)$$

$$Z^* = \frac{R_{gb}}{1+(j\omega\tau_{gb})^{1-\alpha}} \quad (5)$$

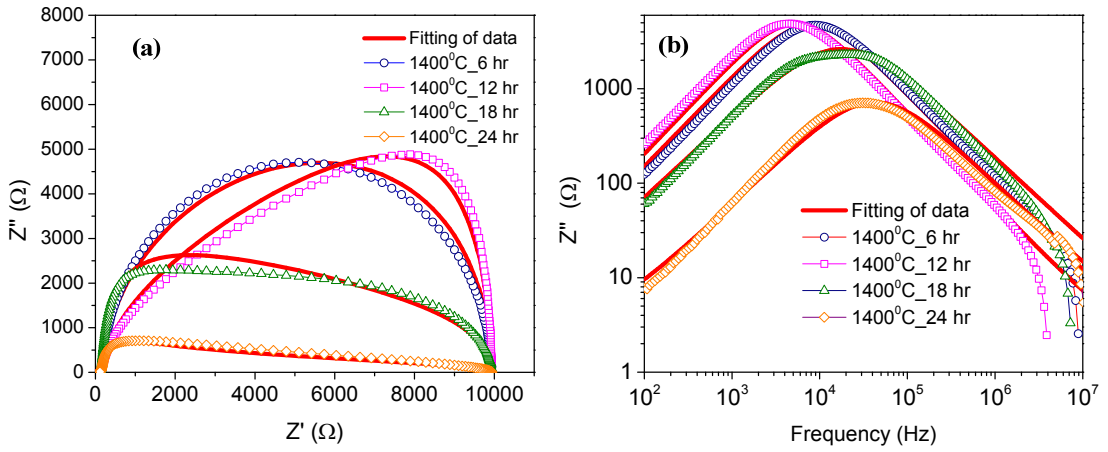


**Figure 4** (a) Impedance spectra as a function of sintering time. Solid curves are the best fits to Eq. (5), (b) Frequency dependence of $Z''$and solid curves.

**Figure 4(b)** shows the frequency dependence of $Z''$ in the imaginary part of complex impedance ($Z^*$) at high temperature (1400 °C) of sintering time from 6 to 24 h and the solid curves are the best fits to the Cole-Cole equation. It was observed that each sintering time exhibits a different shifted imaginary impedance ($Z''$), shifting dramatically to higher frequency as sintering time increases. However, the intensity of ($Z''$) decreases as the sintering time increases. As discussed in the previous section, both electrical responses are thermally activated. Based on Eq. (3), the response peak of the grains and grain boundaries are positioned at $1/(2\pi R_g C_g)$ and $1/(2\pi R_{gb} C_{gb})$, respectively, and the peak values are proportional to the associated resistances. Generally, the peak frequency for grain boundaries is much lower than that for grains due to their large resistance and capacitance compared with those of grains. **Figure 4(a)** shows the impedance spectra for the $Y_2NiMnO_6$ ceramics at high temperature and different

sintering time. It can be seen that the impedance semicircles consist of 4 semicircles, which have different characteristics with each condition. They can be slightly separated at the beginning of the $Z'$ axis for the different sintering time. Subsequently, impedance values increased dramatically and separated clearly in lower impedance region. Consequently, in the impedance spectra, we found that the small semicircle at 24 h, which corresponds to the low intensity and weak peak in **Figure 4(b)**, while the large semicircle at 12 h shows a high intensity and strong peak. Furthermore, in the part of capacitances and resistance in grain and grain boundary are summarized in **Table 1** and **Figure 5**. It is noted that the capacitance values in the grain boundary are larger than in the grain interior for sintering time at 12 and 18 h, and the resistance increases significantly.

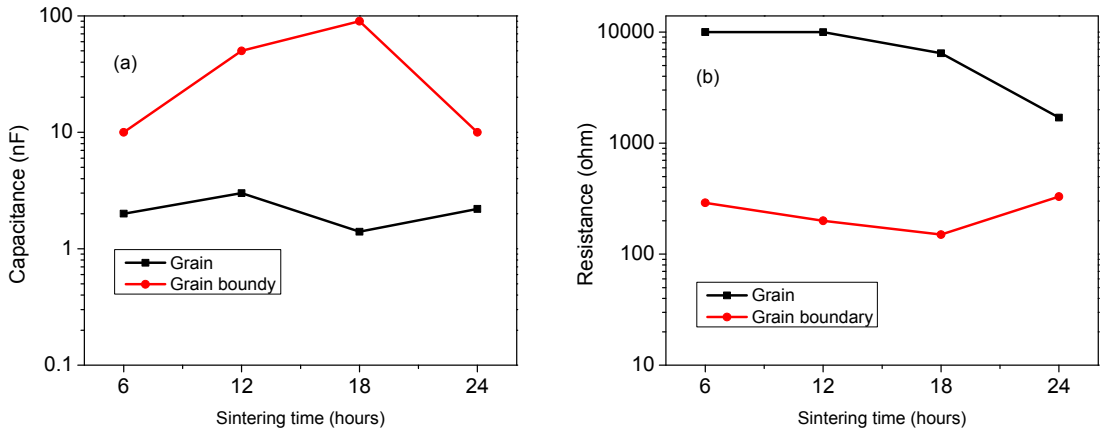


**Figure 5** (a) Sintering time dependence of capacitance and (b) resistance.

**Table1** Activation energies of grain and grain boundary of the $Y_2NiMnO_6$ ceramics.

| Sample (1400 °C) | Activation energy (eV) | | | |
|---|---|---|---|---|
| | $E_a(\tau_g)$ | $\alpha g$ | $E_a(\sigma_{gb})$ | $\alpha gb$ |
| 6 hours | 0.172 | 0.960 | 0.359 | 0.015 |
| 12 hours | 0.309 | 0.980 | 0.451 | 0.015 |
| 18 hours | 0.331 | 0.870 | 0.545 | 0.015 |
| 24 hours | 0.381 | 0.890 | 0.626 | 0.015 |

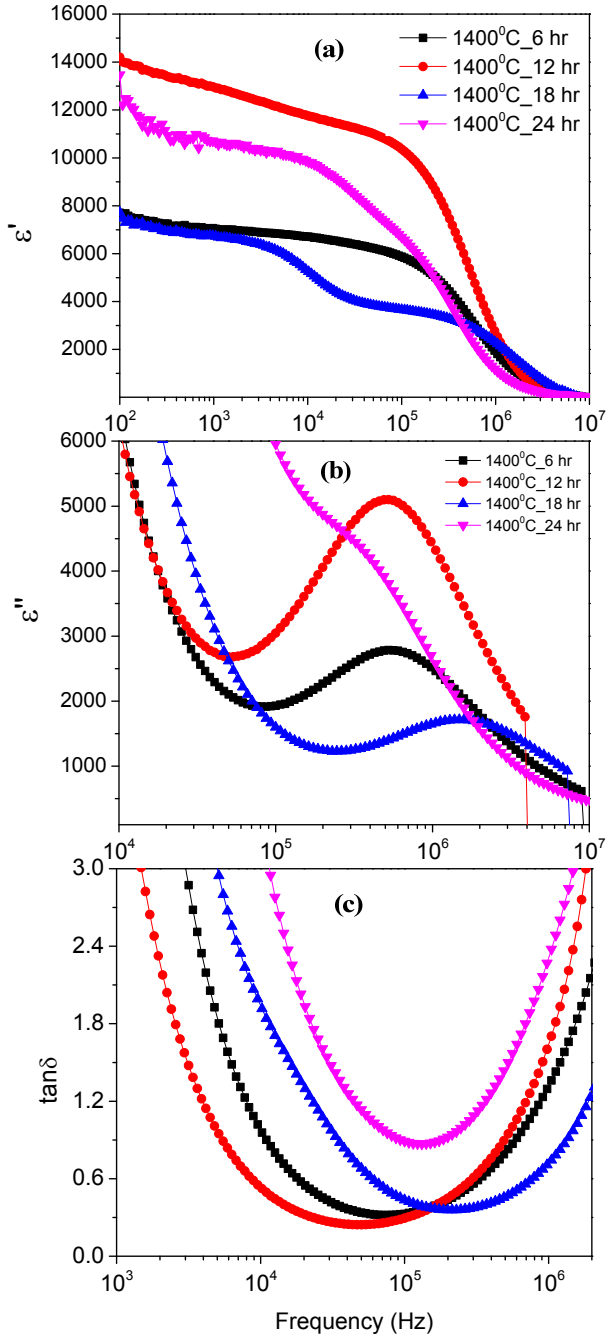


**Figure 6** Frequency dependence of dielectric properties of $Y_2NiMnO_6$ ceramics with different sintering time obtained from Debye and Cole-Cole relaxation models.

**Figure 6** shows the dielectric properties that consist of dielectric permittivity ($\varepsilon'$) (a), dielectric loss ($\varepsilon''$) (b) and loss tangent ($\tan\delta$) (c) of $Y_2NiMnO_6$ ceramics as a function of temperature under bias at 30 °C for several frequencies. According to the data, the values of $\varepsilon' \sim 1.420x10^4$ for sintered time at 12 h and $\sim 1.346x10^4$ for 24 h at low frequency ($10^2$ Hz), respectively. Interestingly, they decreased significantly at higher frequency for all sintered times. On the other hand, the highest peak position had a value of $\varepsilon'' \sim 5.101x10^3$ at 12 h and a low value of $\sim 1.405x10^3$ at 18 h, it was observed that after $\varepsilon'$ plummeted rapidly at high frequency the appearance of a corresponding relaxation peak in the $\varepsilon''$ followed. Consequently, we found that the relaxation peak had a shifted peak at high frequency for long sintering times. Therefore, the change in dielectric properties of the sintered $Y_2NiMnO_6$ ceramics can be correlated to microscopic changes in microstructure of ceramics such as an improvement of $\varepsilon'$ is attributed to an increase in grain size, as shown in **Figure 2**. However, to understand the possible mechanism and behavior associated with decreasing dielectric permittivity and sintering time we have explored the Cole-Cole relaxation model. Normally, a dielectric relaxation in ceramic materials can be empirically described by a Cole-Cole relaxation model, the modified Debye Eq. (6). This is given by;

$$\varepsilon^* = \varepsilon' - j\varepsilon'' = \varepsilon_\infty + \left[\left(\frac{\varepsilon_S - \varepsilon_\infty}{1+(j\omega\tau)^\alpha}\right)\right] \quad (6)$$

where, $\varepsilon_s$ is the static frequency, $\varepsilon_\infty$ is the high frequency limit of dielectric permittivity and the dielectric relaxation is $\tau$, $\omega$ is the angular frequency, which is includes a constant value $\alpha$ ($0 \leq \alpha \leq 1$) only. For an ideal Debye relaxation, $\alpha = 1$, ($\alpha = 0$ corresponds to the standard Debye relaxation). At the same time, $\alpha < 1$, implies that the relaxation has a distribution of relaxation time, leading to a broader peak shape than a Debye peak. As seen in **Figures 6(a) - 6(d)**, both low frequency and high frequency parts can be well fitted by the Cole-Cole relaxation model. Consequently, the $\alpha$ values of temperature with 200 to 140 °C at ~0.864 (for 1400 °C at 24 h), while the high $\alpha$ values at 6 h of about $\sim 0.982$, respectively. In addition the $Y_2NiMnO_6$ ceramics were measured over a temperature range from 200 to −50 °C, important for diverse applications. However, the loss tangent in our samples is very high value at long sintering times and increases at low frequency.

By fitting the results, the mean relaxation times ($\tau$) at different temperatures (200 to −50 °C) were obtained. It was found that the temperature dependence of the fitted $\tau$ values for sintering time follow the Arrhenius law;

$$\tau = \tau_0 \exp\left(\frac{E_a}{k_B T}\right) \quad (7)$$

where $\tau_0$ is a pre-factor, $E_a$ is the activation energy required for the relaxation process, $k_B$ is Boltzmann constant, and T is the absolute temperature. The curves fitted using Eq. (7), as illustrated in the inset (a-d) of **Figure 7**. Furthermore, we have also found that the activation energy $E_{a(\tau g)}$ value of the relaxation in the grain is 0.172, 0.309, 0.331 and 0.381 eV, for sintering times 6, 12, 18 and 24 h, respectively. However, the value of $E_{a(\tau gb)}$ for relaxation in the grain boundary at long sintering times is about 0.407 eV. It was observed that the activation energy for the relaxation is consistent with the loss of the dielectric peak, as shown in **Figure 6(b)**. On the other hand, in this work we investigated the conduction activation energy. As demonstrated in **Table 1**, we found values of $E_{a(\sigma gb)}$ for the conduction activation energy in the grain boundary of 0.359, 0.451, 0.545 and 0.626 eV at 6, 12, 18 and 24 h, accordingly. As previously reported, the polarization relaxation has a close relationship to the conductivity in the grain boundary, whereas the conduction activation energy in the grain interior does not correspond to the $Y_2NiMnO_6$ ceramic.

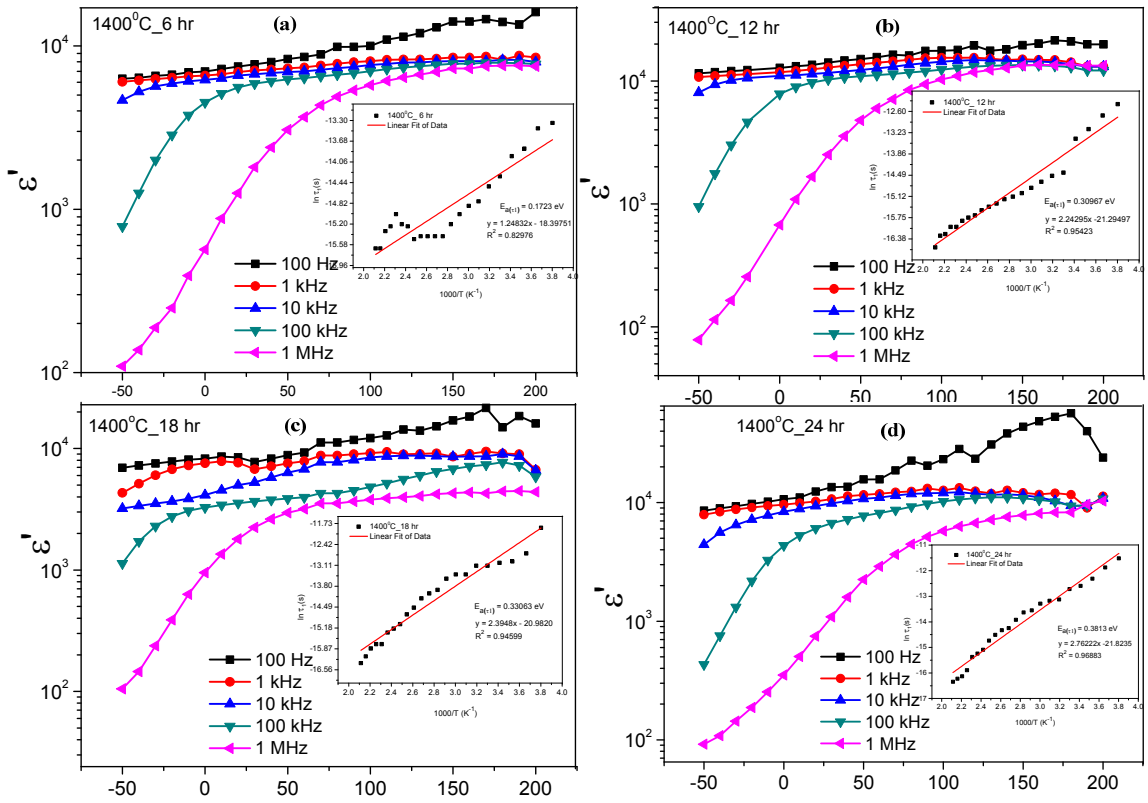


**Figure7** The temperature dependence of dielectric permittivity; inset shows temperature dependence of relaxation time for materials sintered at 1400 °C for (a) 6 h, (b) 12 h, (c) 18 h and (d) 24 h.

## Conclusions

In summary, $Y_2NiMnO_6$ ceramics were prepared by thermal decomposition and sintering. XRD results show the main phase of $Y_2NiMnO_6$, confirming the different sintering times. Interestingly, the grain sizes showed significant growth with sintering time, as indicated by SEM. The values of high $Z' \sim 1.02 \times 10^4$ Ω, $R_g \sim 1.0 \times 10^4$ Ω and $C_{gb} \sim 90$ nF, using a bias temperature at 30 °C, respectively. It was measured by using temperature range 200 to −50 °C in order to investigate the dielectric properties associated with a heating bias inside the materials. We found that the dielectric permittivity had high values at low frequency, while at high frequency low dielectric permittivities were found at one temperature.

## Acknowledgments

The authors would like to thank the Commission of Higher Education, Ministry of Education of Thailand for the financial support. The authors also thank the Advanced Materials Physics Laboratory (Amp.), School of Physics, Institute of Science, Suranaree University of Technology, Nakhon Ratchasima and the division of Industrial Materials Science, Faculty of Science and Technology, Rajamangala University of Technology Phra Nakhon (RMUTP).

**References**

[1] J Wu, CW Nan, Y Lin and Y Deng. Giant dielectric permittivity observed in Li and Ti doped NiO. *Phys. Rev. Lett.* 2002; **89**, 217601.
[2] JB Wu, J Nan, CW Nan, Y Lin, Y Deng and S Zhao. Analysis of AC electrical properties of (Li and Ti) doped NiO. *Mater. Sci. Eng. B* 2003; **99**, 294-7.
[3] F Amaral, LC Costa and MA Valente. Decrease in dielectric loss of $CaCu_3Ti_4O_{12}$ by the addition of $TiO_2$. *J. Non-Cryst. Solids* 2011; **357**, 775-81.
[4] EA Patterson, S Kwon and CC Huang. Effects of $ZrO_2$ additions on the dielectric properties of $CaCu_3Ti_4O_{12}$. *Appl. Phys. Lett.* 2005; **87**, 182911-3.
[5] Z Yang, L Zhang, X Chao, L Xiong and J Liu. High permittivity and low dielectric loss of the $Ca_{1-x}Sr_xCu_3Ti_4O_{12}$ ceramics. *J. Alloys Compd*. 2011; **509**, 8716-9.
[6] CM Wang, SY Lin, KS Kao, YC Chen and SC Weng. Microstructural and electrical properties of $CaTiO_3$-$CaCu_3Ti_4O_{12}$ ceramics. *J. Alloys Compd.* 2010; **491**, 423-30.
[7] L Ramajo, R Parraa, JA Varela, MM Reboredo, MA Ramire and MS Castro. Influence of vanadium on electrical and microstructural properties of $CaCu_3Ti_4O_{12}$/$CaTiO_3$. *J. Alloys Compd.* 2010; **497**, 349-53.
[8] S Kumar, G Giovannetti, JVD Brink and S Picozzi. Theoretical prediction of multiferroicity in double perovskite $Y_2NiMnO_6$. *Phys. Rev*. 2010; **82**, 134429.
[9] RJ Booth, R Fillman, H Whitaker, A Nag, RM Tiwari, KV Ramanujachary, J Gopalakrishnan and SE Lofland. An investigation of structural, magnetic, and dielectric properties of $R_2NiMnO_6$ (R=rare earth, Y). *Mater. Res. Bull*. 2009; **44**, 1559-64.
[10] M Mouallem-Bahout, T Roisnel, G Andre, D Gutierrez, C Moure and O Pena. Nuclear and magnetic order in $Y(Ni,Mn)O_3$ manganites by neutron powder diffraction. *Solid State Comm*. 2004; **129**, 255-60.
[11] KD Chanadrsekhar, AK Das and A Venimadhav. Magnetic properties of $La_2NiMnO_6$ nanoparticles. *Solid State. Phys.* 2012; **1447**, 1237-38.
[12] YQ Lin, XM Chen and XQ Liu. Relaxor-like dielectric behavior in $La_2NiMnO_6$ double perovskite ceramics. *Solid State Comm*. 2009; **149**, 784-7.
[13] WZ Yang, MM Mao, XQ Liu and XM Chen. Structure and dielectric relaxation of double-perovskite $La_2CuTiO_6$ ceramics. *J. Appl. Phys*. 2010; **107**, 124102.
[14] JV den Brink and DI Khomskii. Multiferroicity due to charge ordering. *J. Phys. Condens. Matter*. 2008; **20**, 434217.
[15] DJ Singh and CH Park. Polar behavior in a magnetic perovskite from a-site size disorder: A density functional study. *Phys. Rev. Lett*. 2008; **100**, 087601.
[16] MT Anderson, KB Greenwood, GA Taylor and R Poeppelmeier. B-cation arrangement in double perovskites. *Prog. Solid State Chem*. 1993; **22**, 197-233.
[17] MP Singh, KD Truong, S Jandl and P Fournier. Magnetic properties and phonon behavior of $Pr_2NiMnO_6$ thin films. *Appl. Phys. Lett*. 2011; **98**, 162506.
[18] K Yoshii, N Ikeda and M Mizumaki. Magnetic and dielectric properties of the ruthenium double perovskites $La_2MRuO_6$ (M=Mg, Co, Ni, and Zn). *Phys. Status Solidi A* 2006; **203**, 2812-7.
[19] Y Hiramitsu, K Yoshii, Y Yoneda, J Mizuki, A Nakamura, Y Shimojo, Y Ishii, Y Morii and N Ikeda. Magnetic and dielectric properties of $Tb_{0.5}Ca_{0.5}MnO_3$. *Jpn. J. Appl. Phys.* 2007; **46**, 7171-4.
[20] CR Serrao, A Sundaresan and CNR Rao. Multiferroic nature of charge-ordered rare earth manganites. *J. Phys. Condens. Matter. Lett*. 2007; **9**, 496217.
[21] JR Sahu, CR Serrao, A Ghosh, A Sundaresan and CNR Rao. Charge-order-driven multiferroic properties of $Y_{1-x}Ca_xMnO_3$. *Solid State Comm.* 2009; **149**, 49-51.
[22] DV Efremov, JVD Brink and DI Khomskii. Bond-versus site-centred ordering and possible ferroelectricity in manganites. *Nat. Mater*. 2004; **21**, 853-6.
[23] S Theeranum, CH Naphat, M Chivalrat and Y Teerapon. Synthesis, characterization, and dielectric properties of $Y_2NiMnO_6$ ceramics prepared by a simple thermal decomposition route. *J. Mater. Sci. Mater. Electron*. 2014; **25**, 1361-8.

[24] DC Sinclair and AR West. Impedance and modulus spectroscopy of semiconducting $BaTiO_3$ showing positive temperature coefficient of resistance. *J. Appl. Phys*. 1989; **66**, 3850-6.
[25] RW West, TB Adams, FD Morrisom and DC Sinclair. Novel high capacitance materials:- $BaTiO_3$:La and $CaCu_3Ti_4O_{12}$. *J. Eur. Ceram. Soc*. 2004; **24**, 1439-48.
[26] J Liu, CG Duan, WN Mei, RW Smith and JR Hardy. Dielectric properties and Maxwell-Wagner relaxation of compounds $ACu_3Ti_4O_{12}$ (A=Ca, Bi2/3, Y2/3, La2/3). *J. Appl. Phys*. 2005; **98**, 093703.